Dust mobilization in the presence of magnetic fields

Li Hsia Yeo ,[*] Noah Hood ,[†] Xu Wang , and Mihály Horányi
Laboratory for Atmospheric and Space Physics, University of Colorado, Boulder, Colorado 80303, USA

We present a study of surface dust mobilization due to photoelectric charging in the presence of a magnetic field. Dust mobilization is observed to be inhibited in certain regions and is correlated with the orientation of the magnetic field. The recent patched charge model, which describes a mechanism for dust charging and mobilization, is extended to explain the effects of magnetic fields seen in our laboratory results. We propose that ambient electrons collected in photoemitting areas precipitate changes in the emission and reabsorption of photoelectrons inside microcavities between dust grains. This affects the charging, repulsion, and subsequent mobilization of the dust grains surrounding the microcavities. The magnetic field controls the movement of ambient electrons across the dusty surface, resulting in active and inactive regions of dust mobilization. Computer simulations show that regions of ambient electron accumulation as imposed by the magnetic field match the areas of high dust activity.

The electrostatic lofting of dust as driven by ultraviolet (UV) radiation and the solar wind plasma is thought to be the physical process behind several observed phenomena on many airless bodies in our solar system. The earliest of these was the lunar horizon glow, a diffuse scattering of light above the Moon's horizon seen in images captured by the Surveyor 5, 6, and 7 spacecraft [1–3]. Observations of dust ponds on the surfaces of the asteroid Eros [4] and the Comet 67P [5] suggest electrostatic transport of dust in the absence of water flow or wind. The "spokes" in Saturn's rings [6,7] are thought to be footprints of electrostatically lofted dust above the ring plane. The lack of fine-grained material on the surfaces of the asteroids Bennu and Ryugu has been proposed to be due to electrostatic escape of small grains [8].

On Earth, interest in dust charging and lofting in plasma environments has been widespread due to its applicability in fusion [9–11] and semiconductor fabrication [12–14] devices where particulate contamination has been identified as an adverse problem.

Early experimental work [15,16] demonstrated dust release from a surface exposed to plasma, and subsequent experiments [17–20] investigated dust charging, mobilization, and lofting in various plasma environments. A charge fluctuation theory showed temporal increases of the dust charge as a result of stochastic processes of electrons and ions hitting the surface [16,21–23]. However, when a dust grain was treated as part of the surface, the expected accumulated charge was shown to be far too small to cause its lofting [16], even considering various possible enhanced charging effects of a dust grain resting on a solid surface [24]. All these models were based on the charging processes and electric fields in the plasma sheath above the dusty surface.

Recent laboratory work [25,26] advanced our understanding of the physical processes underlying dust charging and lofting in a plasma and/or under UV radiation by recognizing the role of cavities that form between dust particles. The patched charge model (PCM) [25] describes a microscale charging process within the dusty surface. It proposes that the emitted photo or secondary electrons can be reabsorbed inside intergrain microcavities, causing substantial buildups of negative charges on adjacent grains. These negative charges can be several orders of magnitude larger than what earlier surface charging models predict [26]. The buildup of large charges on a grain scale was also verified by computer simulations [27]. It was found that lofting velocities are dependent on the grain size [28], lofting rates decrease as a function of time [29], and smaller grains are more easily lofted [30]. Once lofted, the subsequent dust dynamics depend on dust size, the properties of the plasma sheath, and gravity [31,32].

To date, the PCM has yet to be applied in the presence of magnetic fields. On the Moon, high-albedo markings, known as lunar swirls, are colocated with lunar magnetic anomalies (LMAs) [33,34]. It has been suggested that electrostatically lofted dust is re-sorted by surface electric fields created by solar wind interactions with LMAs [35–41], forming high-albedo patterns due to the increased brightness of fine dust [42]. Understanding dust charging, mobilization, and transport in the presence of magnetic fields is also of interest in the development of efficient dust mitigation approaches for plasma facilities that incorporate magnetic fields, such as tokamak fusion devices [11] and plasma processing in semiconductor manufacturing [13], as well as any human or robotic exploration of LMA regions.

In this Letter, we present both experimental work showing the behavior of dust grains in the presence of a dipole magnetic field as well as computer simulation results that reveal

---

*Now at Goddard Space Flight Center, MD 20771, Maryland; li.yeo@colorado.edu
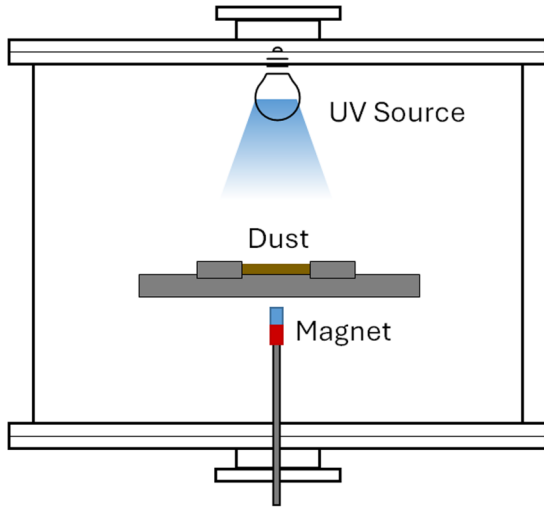†Now at the University of California, San Diego, CA 92182.

FIG. 1. Schematic of the experimental setup. A circular bed 4 cm in diameter and 1-mm deep of Martian simulant dust (<38 microns in diameter) is placed on an insulating plate in a vacuum chamber. A permanent magnet is placed underneath the dust bed. The dust is irradiated and charged by UV light (172 nm or 7.2 eV).

the underlying physics driving the dust activity as understood by an extended PCM.

The experiment was performed in a vacuum chamber 50 cm in diameter and 28-cm tall (Fig. 1). A permanent dipole magnet with a maximum field strength of ∼1.2 kG at its surface was placed under a circular bed of Martian regolith simulant [43]. The bed was 4 cm in diameter and 1-mm deep, whereas the dust size was no larger than 38 μm. Under a vacuum base pressure of 10^{-6} torr, the dusty surface was irradiated with UV light at 172 nm (i.e., 7.2 eV).

For reference, this setup is compared to LMAs (<1 km) with field strengths of ∼1000 nT. Important dimensionless parameters, such as the ratios of the electron gyroradius and Debye length to the length scale of the magnetic fields are comparable (Table I). However, the ratios of the electron gyroradius to the Debye length, which indicate the relative strengths of the magnetic field and the near-surface electric fields as experienced by electrons, are not comparable between the two cases. These values are calculated using lunar photoelectron characteristics from Refs. [44,45] for typical solar activity levels during the day. Photoelectron characteristics in the laboratory are referenced from Ref. [46].

TABLE I. Comparison of LMA and laboratory parameters. Approximate ratios of the electron gyroradius r_g and Debye length λ_D to the length scale L of the magnetic field are shown for the case of an LMA (<1 km with field strength of ∼1000 nT) and the laboratory setup. The ratio of the gyroradius to the Debye length is also shown for both scenarios.

	LMA	Laboratory
r_g/L	≪1 (3 m/1 km)	≪1 (0.1 mm/5 cm)
λ_D/L	≪1 (1 m/1 km)	<1 (2 cm/5 cm)
r_g/λ_D	>1 (3 m/1 m)	≪1 (0.1 mm/2 cm)

The dust movement was recorded using a digital video camera with a frame rate of 1 fps. A frame-by-frame analysis was performed on the footagewhere images were converted into gray scale, and changes in the pixel brightness between consecutive frames were used as a measure of dust activity.

The magnet was placed 5 mm below the dust bed with the dipole moment perpendicular or parallel to the surface, resulting in a maximum field strength of ∼200 G at the surface of the dust bed. Dust activity was found to be correlated with the orientation of the magnet. When the dipole moment was perpendicular to the surface, dust activity was concentrated in a circular spot directly above the magnetic cusp as well as in a large ring at the edge of the dust bed, whereas the dipole lobe region showed no dust mobilization [Fig. 2(a)]. When the dipole moment was parallel to the surface, the observed pattern was asymmetric inside the dust ring with one side of the lobe region active and the other side inhibited [Fig. 2(b)]. When the parallel dipole moment was reversed, the dust activity pattern was observed to flip about the dipole axis.

We rule out direct interactions between the dust grains and the magnetic field as an explanation for these observations for two reasons: (1) the dust grains do not consist of ferromagnetic materials; and (2) the charge-to-mass ratios of the dust grains are too small for them to be affected by the magnetic field. Given the maximum field strength of ∼200 G at the surface of the dust bed and initial lofting conditions measured by ref. [26], the minimum gyroradii of the dust grains are on the order of kilometers. Additionally, the minimum gyroradii of the photoelectrons are ∼125 μm, larger than the dimensions of the microcavities, which are on the order of the grain size (<38 μm). Therefore, it is expected that the magnetic field has a minimal effect on the emission and reabsorption of photoelectrons inside the microcavities, but it remains critical in shaping the large-scale motion of the ambient photoelectrons above the surface.

To explain these observations, an extension to the PCM is suggested. The original PCM [25] describes a potential barrier across a microcavity created between grains that emit and collect photoelectrons (Fig. 3). The magnitude of the potential barrier is determined by the energy distribution of the photoelectrons. The extended PCM suggests that ambient electrons above the dusty surface, (e.g., photoelectrons emitted from neighboring areas) can control the emission and subsequent reabsorption of photoelectrons inside microcavities. When ambient electrons are collected by a positively charged photoemitting surface [Fig. 3(a), the surface potential is lowered. This causes the emission of more photoelectrons and the accumulation of more negative charges on the surrounding grains to maintain the same equilibrium potential barrier across the microcavity [Fig. 3(b)]. Subsequently, repulsive forces between these negatively charged grains are increased, resulting in substantial dust activity. Conversely, photoemitting dust grains in microcavities that do not receive ambient electrons emit fewer photoelectrons, causing the surrounding grains to collect fewer negative charges and remain immobilized.

As a test of the extended PCM, a forward Monte Carlo test particle computer simulation [47] was performed that tracked the trajectories of 80 000 ambient electrons photoemitted from the dusty surface and the vacuum chamber walls. The bulk
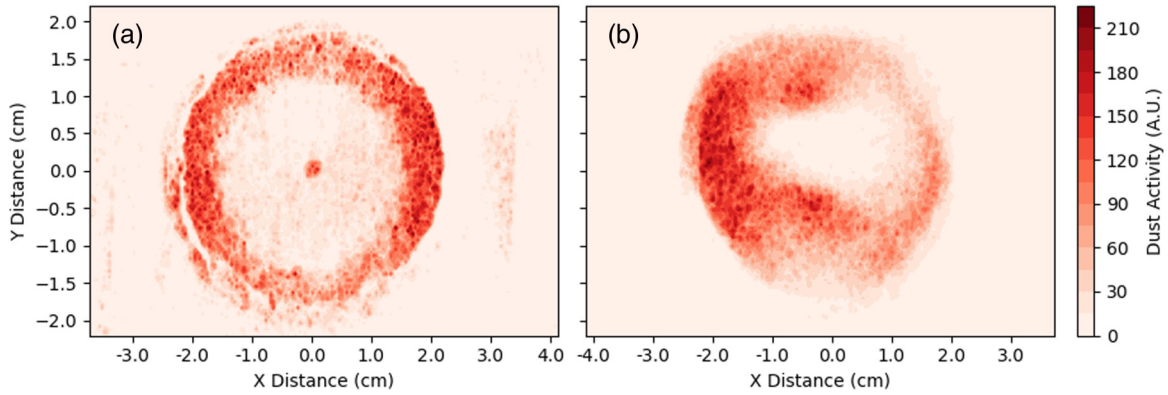
FIG. 2. Dust activity profiles. Dust activity levels extracted from recorded images when the dipole magnet is a) perpendicular and (b) parallel to the dust surface. The center of the magnet are 7.5 and 10.5 mm away from the dust surface, respectively.

dusty surface was assumed to be charged positively due to photoemission. The sheath electric field was assumed to be 10 V/m at the surface and to decay with a Debye length of 2 cm [46]. An ideal magnetic dipole closely matching the measured magnetic field above the dusty surface was used in the simulation (Fig. 4). The dipole moment was $M = 5.54 \times 10^{-9}$ Am^2. In a simulation space of $8 \times 8 \times 3$ cm, individual electrons with energies of 0.5 eV [48] were emitted from the bottom dusty surface or a wall with a random initial direction and subjected to the electric and magnetic fields described above. Particle trajectories were calculated with a time step of 5×10^{-10} s, a fraction of the smallest possible gyroperiod.
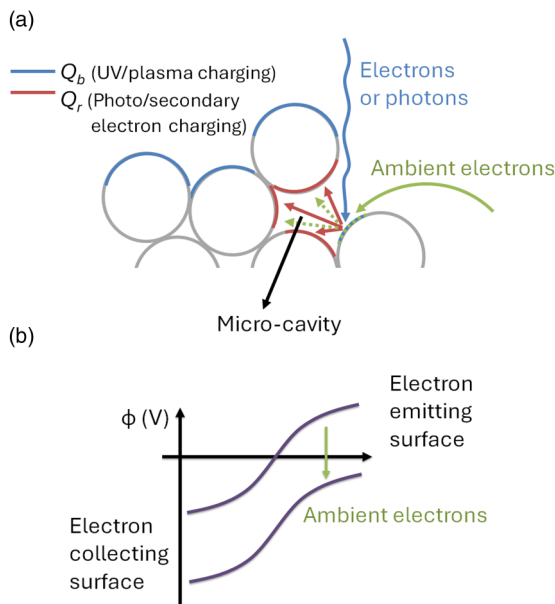

FIG. 3. Extended PCM. (a) Collection of ambient electrons on a photoemitting dust grain within the microcavity is added to the original PCM [25]. (b) The potential barrier created between grains that emit and collect photoelectrons across the microcavity. The collection of ambient electrons causes a downward shift in the potential barrier, indicating more photoemission and, subsequently, increased accumulation of negative charges on the surrounding grains. Repulsive forces between the negatively charged grains are, therefore, increased.

Each trajectory was terminated when the electron crossed the boundary of the simulation space.

Figure 5 shows the landing patterns of ambient electrons generated by the simulations when the dipole moment of an ideal magnet was (a) perpendicular and (b) parallel to the dusty surface. The center of the dipole was at 8 and 10 mm below the surface, respectively. For photoelectrons emitted from the dusty surface, only those that moved, at least, 4 mm from where they originated were included in the landing patterns. Photoelectrons that moved no further than 4 mm were considered to be immobile and were excluded. This resulted in 12.2% and 7.3% of photoemitted electrons being excluded from the vertically and horizontally oriented dipole simulations respectively. This distance threshold was defined from the gyroradii (~3 mm) of electrons at the edge of the dust bed (i.e., >2 cm from the center) where dust was active. The landing patterns within the circular area of the dust bed (Fig. 5) show a match with the observed dust active regions (Fig. 2).

When the dipole moment was perpendicular to the surface [Fig. 5(a)], ambient electrons were funneled into the cusp region above the center of the dipole. Furthermore, from the cusp (>2 cm), the magnetic field strength is weaker so that ambient electrons with gyroradii >3 mm could move
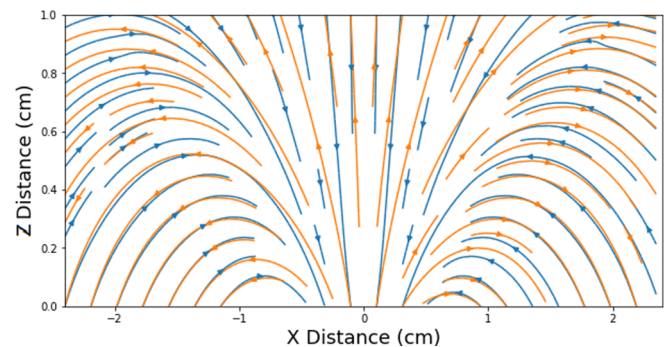

FIG. 4. Measured and simulated magnetic fields. Magnetic field lines measured from the permanent magnet (blue) and from the theoretical dipole (orange). At the origin, which corresponds to the center of the surface of the permanent magnet, the magnetic field strengths of both are 1.2 kG.
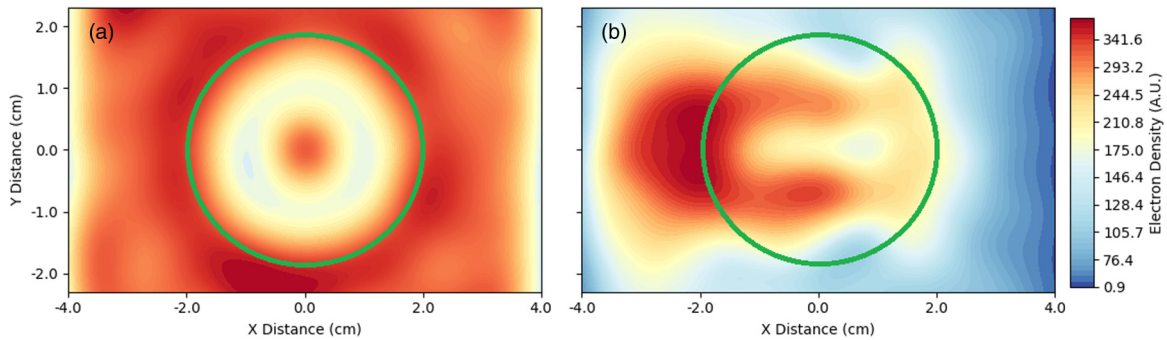
FIG. 5. Simulated electron landing patterns. Electron landing patterns generated by the simulations when the magnetic dipole moment is (a) perpendicular and (b) parallel (along the *Y* axis) to the surface. The dipoles are placed right below the origin. The green circles indicate the area of the dust bed in the experiment.

more freely. In these two regions, dust was active as shown in Fig. 2(a). In contrast, the dipole lobe region showed little dust activity because the ambient electrons were unable to move across the magnetic field lines to reach this region.

When the dipole moment was parallel to the surface [Fig. 5(b)], the ambient electrons were concentrated in the two cusp regions, as well as on one side of the dipole lobe due to the $E \times B$ drift. This resulted in an asymmetric landing pattern that is in agreement with the dust activity shown in Fig. 2(b). When the dipole moment was reversed, the $E \times B$ drift moved in the opposite direction, resulting in a landing pattern that is flipped about the dipole axis and found to be consistent with observed dust activity.

The expanded PCM emphasizes the role of the supply of ambient electrons in ensuring the charge buildup within microcavities and the subsequent mobilization of dust grains, complementing our understanding of the physics of dust charging and mobilization. With regards to LMAs, the

parameters shown in Table I indicate that lunar crustal magnetic fields have weaker effects on the motion of photoelectrons. Electric fields created as a result of solar wind interactions with LMAs [49–51] may have a bigger role in redistribution of the photoelectrons, thereby influencing dust charging and lofting in these regions and resulting in resorting and subsequent albedo patterns related to the formation of lunar swirls. The effect presented in this Letter should be considered in future model developments in addition to other existing swirl-formation mechanisms. Our results indicate that strong magnetic fields in fusion devices and semiconductor manufacturing processes, such as magnetron sputtering are expected to have significant effects on the charging, mobilization, and transport of dust.

[1] D. Criswell, Horizon-glow and the motion of lunar dust, Photon and Particle Interactions with Surfaces in Space **37**, 545 (1973).

[2] J. Rennilson and D. R. Criswell, Surveyor observations of lunar horizon-glow, Moon **10**, 121 (1974).

[3] J. E. Colwell, S. Batiste, M. Horányi, S. Robertson, and S. Sture, Lunar surface: Dust dynamics and regolith mechanics, Rev. Geophys. **45**, RG2006(R) (2007).

[4] M. S. Robinson, P. C. Thomas, J. Veverka, S. Murchie, and B. Carcich, The nature of ponded deposits on eros, Nature (London) **413**, 396 (2001).

[5] N. Thomas, B. Davidsson, M. R. El-Maarry, S. Fornasier, L. Giacomini, A. G. Gracia-Berná, S. F. Hviid, W.-H. Ip, L. Jorda, H. U. Keller, J. Knollenberg, E. Kührt, F. L. Forgia, I. L. Lai, Y. Liao, R. Marschall, M. Massironi, S. Mottola, M. Pajola, O. Poch, et al., Redistribution of particles across the nucleus of comet 67p/churyumov-gerasimenko, Astron. Astrophys. **583**, A17 (2015).

[6] B. A. Smith, L. Soderblom, R. Beebe, J. Boyce, G. Briggs, A. Bunker, S. A. Collins, C. J. Hansen, T. V. Johnson, J. L. Mitchell, R. J. Terrile, M. Carr, A. F. Cook, J. Cuzzi, J. B. Pollack, G. E. Daneilson, A. Ingersoll, M. E. Davies, G. E. Hunt, H. Masursky *et al.*, Encounter with saturn: Voyager 1 imaging science results, Science **212**, 163 (1981).

[7] G. Morfill, E. Grün, C. Goertz, and T. Johnson, On the evolution of saturn's "spokes": Theory, Icarus **53**, 230 (1983).

[8] H. Hsu, X. Wang, A. Carroll, N. Hood, and M. Horanyi, Electrostatic removal of fine-grained regolith on sub-km asteroids, in *AAS/Division for Planetary Sciences Meeting Abstracts*, AAS/Division for Planetary Sciences Meeting Abstracts (AAS, Washington, D.C., 2020), Vol. 52, p. 402.06.

[9] J. Winter, Dust in fusion devices - experimental evidence, possible sources and consequences, Plasma Phys. Controlled Fusion **40**, 1201 (1998).

[10] A. Y. Pigarov, S. I. Krasheninnikov, T. K. Soboleva, and T. D. Rognlien, Dust-particle transport in tokamak edge plasmas, Phys. Plasmas **12**, 122508 (2005).

[11] S. I. Krasheninnikov, R. D. Smirnov, and D. L. Rudakov, Dust in magnetic fusion devices, Plasma Phys. Controlled Fusion **53**, 083001 (2011).

[12] G. S. Selwyn, J. Singh, and R. S. Bennett, In situ laser diagnostic studies of plasma-generated particulate contamination, J. Vacuum Sci. Technol. A**7**, 2758 (1989).

[13] G. S. Selwyn, J. E. Heidenreich, and K. L. Haller, Particle trapping phenomena in radio frequency plasmas, Appl. Phys. Lett. **57**, 1876 (1990).

[14] V. E. Fortov, A. G. Khrapak, S. A. Khrapak, V. I. Molotkov, and O. F. Petrov, Dusty plasmas, Phys. Usp. **47**, 447 (2004).

[15] T. E. Sheridan, J. Goree, Y. T. Chiu, R. L. Rairden, and J. A. Kiessling, Observation of dust shedding from material bodies in a plasma, J. Geophys. Res.: Space Phys. **97**, 2935 (1992).

[16] T. M. Flanagan and J. Goree, Dust release from surfaces exposed to plasma, Phys. Plasmas **13**, 123504 (2006).

[17] X. Wang, M. Horányi, and S. Robertson, Experiments on dust transport in plasma to investigate the origin of the lunar horizon glow, J. Geophys. Res.: Space Phys. **114** (2009).

[18] X. Wang, M. Horányi, and S. Robertson, Investigation of dust transport on the lunar surface in a laboratory plasma with an electron beam, J. Geophys. Res.: Space Phys. **115**, n/a (2010).

[19] X. Wang, M. Horányi, and S. Robertson, Dust transport near electron beam impact and shadow boundaries, Planet. Space Sci. **59**, 1791 (2011).

[20] N. Ding, J. Wang, and J. Polansky, Measurement of dust charging on a lunar regolith simulant surface, IEEE Trans. Plasma Sci. **41**, 3498 (2013).

[21] A. A. Sickafoose, Experimental levitation of dust grains in a plasma sheath, J. Geophys. Res.: Atmos. **107**, 1408 (2002).

[22] T. E. Sheridan and A. Hayes, Charge fluctuations for particles on a surface exposed to plasma, Appl. Phys. Lett. **98**, 091501 (2011).

[23] T. E. Sheridan, Charging time for dust grain on surface exposed to plasma, J. Appl. Phys. **113**, 143304 (2013).

[24] L. C. J. Heijmans and S. Nijdam, Dust on a surface in a plasma: A charge simulation, Phys. Plasmas **23**, 043703 (2016).

[25] X. Wang, J. Schwan, H.-W. Hsu, E. Grün, and M. Horányi, Dust charging and transport on airless planetary bodies, Geophys. Res. Lett. **43**, 6103 (2016).

[26] J. Schwan, X. Wang, H.-W. Hsu, E. Grün, and M. Horányi, The charge state of electrostatically transported dust on regolith surfaces, Geophys. Res. Lett. **44**, 3059 (2017).

[27] M. Zimmerman, W. Farrell, C. Hartzell, X. Wang, M. Horanyi, D. Hurley, and K. Hibbitts, Grain-scale supercharging and breakdown on airless regoliths, J. Geophys. Res.: Planets **121**, 2150 (2016).

[28] A. Carroll, N. Hood, R. Mike, X. Wang, H.-W. Hsu, and M. Horányi, Laboratory measurements of initial launch velocities of electrostatically lofted dust on airless planetary bodies, Icarus **352**, 113972 (2020).

[29] N. Hood, A. Carroll, R. Mike, X. Wang, J. Schwan, H.-W. Hsu, and M. Horányi, Laboratory investigation of rate of electrostatic dust lofting over time on airless planetary bodies, Geophys. Res. Lett. **45**, 13 (2018).

[30] N. Hood, A. Carroll, X. Wang, and M. Horanyi, Laboratory measurements of size distribution of electrostatically lofted dust, Icarus **371**, 114684 (2022).

[31] L. H. Yeo, X. Wang, J. Deca, H.-W. Hsu, and M. Horányi, Dynamics of electrostatically lofted dust on airless planetary bodies, Icarus **366**, 114519 (2021).

[32] T. J. Stubbs, R. R. Vondrak, and W. M. Farrell, A dynamic fountain model for lunar dust, Adv. Space Res. **37**, 59 (2006).

[33] D. L. Mitchell, J. S. Halekas, R. P. Lin, S. Frey, L. L. Hood, M. H. Acuña, and A. Binder, Global mapping of lunar crustal magnetic fields by Lunar Prospector, Icarus **194**, 401 (2008).

[34] D. T. Blewett, E. I. Coman, B. R. Hawke, J. J. Gillis-Davis, M. E. Purucker, and C. G. Hughes, Lunar swirls: Examin-

ing crustal magnetic anomalies and space weathering trends, J. Geophys. Res.: Atmos. **116**, (2011).

[35] J. S. Halekas, G. T. Delory, D. A. Brain, D. L. Mitchell, and R. P. Lin, Density cavity observed over a strong lunar crustal magnetic anomaly in the solar wind: A mini-magnetosphere? Planet. Space Sci. **56**, 941 (2008).

[36] X. Wang, M. Horányi, and S. Robertson, Characteristics of a plasma sheath in a magnetic dipole field: Implications to the solar wind interaction with the lunar magnetic anomalies, J. Geophys. Res.: Space Phys. **117**, A06226 (2012).

[37] Y. Futaana, S. Barabash, M. Wieser, C. Lue, P. Wurz, A. Vorburger, A. Bhardwaj, and K. Asumura, Remote energetic neutral atom imaging of electric potential over a lunar magnetic anomaly, Geophys. Res. Lett. **40**, 262 (2013).

[38] J. Deca, A. Divin, G. Lapenta, B. Lembege, S. Markidis, and M. Horanyi, Electromagnetic Particle-in-Cell Simulations of the Solar Wind Interaction with Lunar Magnetic Anomalies, Phys. Rev. Lett. **112**, 151102 (2014).

[39] C. Howes, X. Wang, J. Deca, and M. Horányi, Laboratory investigation of lunar surface electric potentials in magnetic anomaly regions, Geophys. Res. Lett. **42**, 4280 (2015).

[40] M. I. Zimmerman, W. M. Farrell, and A. R. Poppe, Kinetic simulations of kilometer-scale minimagnetosphere formation on the moon, J. Geophys. Res.: Planets **120**, 1893 (2015).

[41] J. Deca, A. Divin, C. Lue, T. Ahmadi, and M. Horányi, Reiner Gamma albedo features reproduced by modeling solar wind standoff, Nat. Commun. Phys. **1**, 12 (2018).

[42] I. Garrick-Bethell, J. W. Head III, and C. M. Pieters, Spectral properties, magnetic fields, and dust transport at lunar swirls, Icarus **212**, 480 (2011).

[43] C. C. Allen, K. M. Jager, R. V. Morris, D. J. Lindstrom, M. M. Lindstrom, and J. P. Lockwood, Jsc mars-1: A martian soil simulant, in *Space 98* (1998), pp. 469–476.

[44] Z. Sternovsky, P. Chamberlin, M. Horanyi, S. Robertson, and X. Wang, Variability of the lunar photoelectron sheath and dust mobility due to solar activity, J. Geophys. Res.: Space Phys. **113**, (2008).

[45] S. I. Popel, A. P. Golub', Y. N. Izvekova, V. V. Afonin, G. G. Dol'nikov, A. V. Zakharov, L. M. Zelenyi, E. A. Lisin, and O. F. Petrov, On the distributions of photoelectrons over the illuminated part of the moon, JETP Lett. **99**, 115 (2014).

[46] A. Dove, M. Horanyi, X. Wang, M. Piquette, A. R. Poppe, and S. Robertson, Experimental study of a photoelectron sheath, Phys. Plasmas **19**, 043502 (2012).

[47] R. Marchand, Test-particle simulation of space plasmas, Commun. Comput. Phys. **8**, 471 (2010).

[48] X. Wang, M. Horányi, and S. Robertson, Plasma probes for the lunar surface, J. Geophys. Res.: Space Phys. **113**, (2008).

[49] J. Deca, A. Divin, B. Lembège, M. Horányi, S. Markidis, and G. Lapenta, General mechanism and dynamics of the solar wind interaction with lunar magnetic anomalies from 3-d pic simulations, J. Geophys. Res.: Space Phys., **120**, 6443 (2015).

[50] J. Deca, A. Divin, X. Wang, B. Lembège, S. Markidis, M. Horányi, and G. Lapenta, Three-dimensional full-kinetic simulation of the solar wind interaction with a vertical dipolar lunar magnetic anomaly, Geophys. Res. Lett. **43**, 4136 (2016).

[51] L. H. Yeo, J. Han, X. Wang, G. Werner, J. Deca, T. Munsat, and M. Horányi, Laboratory simulation of solar wind interaction with lunar magnetic anomalies, J. Geophys. Res.: Space Phys. **127** (2022).